

RESEARCH

Open Access



SMARCA4 controls state plasticity in small cell lung cancer through regulation of neuroendocrine transcription factors and REST splicing

Esther Redin¹, Harsha Sridhar¹, Yingqian A. Zhan², Barbara Pereira Mello¹, Hong Zhong¹, Vidushi Durani^{1,5}, Amin Sabet¹, Parvathy Manoj¹, Irina Linkov³, Juan Qiu⁴, Richard P. Koche², Elisa de Stanchina⁴, Maider Astorkia⁶, Doron Betel^{6,7,8}, Álvaro Quintanal-Villalonga^{1*} and Charles M. Rudin^{1,5*}

Abstract

Introduction Small Cell Lung Cancer (SCLC) can be classified into transcriptional subtypes with distinct degrees of neuroendocrine (NE) differentiation. Recent evidence supports plasticity among subtypes with a bias toward adoption of low-NE states during disease progression or upon acquired chemotherapy resistance. Here, we identify a role for SMARCA4, the catalytic subunit of the SWI/SNF complex, as a regulator of subtype shift in SCLC.

Methods ATACseq and RNAseq experiments were performed in SCLC cells after pharmacological inhibition of SMARCA4. DNA binding of SMARCA4 was characterized by ChIPseq in high-NE SCLC patient derived xenografts (PDXs). Enrichment analyses were applied to transcriptomic data. Combination of FHD-286 and afatinib was tested in vitro and in a set of chemo-resistant SCLC PDXs in vivo.

Results SMARCA4 expression positively correlates with that of NE genes in both SCLC cell lines and patient tumors. Pharmacological inhibition of SMARCA4 with FHD-286 induces the loss of NE features and downregulates neuroendocrine and neuronal signaling pathways while activating non-NE factors. SMARCA4 binds to gene loci encoding NE-lineage transcription factors ASCL1 and NEUROD1 and alters chromatin accessibility, enhancing NE programs. Enrichment analysis applied to high-confidence SMARCA4 targets confirmed neuron related pathways as the top GO Biological processes regulated by SMARCA4 in SCLC. In parallel, SMARCA4 also controls REST, a known suppressor of the NE phenotype, by regulating SRRM4-dependent *REST* transcript splicing. Furthermore, SMARCA4 inhibition drives ERBB pathway activation in SCLC, rendering SCLC tumors sensitive to afatinib.

Conclusions This study nominates SMARCA4 as a key regulator of the NE state plasticity and defines a novel therapeutic strategy for SCLC.

Keywords Lung Cancer, SCLC, Plasticity, Epigenetics, Targeted therapies

Lead Contact: Charles M. Rudin

*Correspondence:

Álvaro Quintanal-Villalonga

quintaa@mskcc.org

Charles M. Rudin

rudinc@mskcc.org

Full list of author information is available at the end of the article



© The Author(s) 2024. **Open Access** This article is licensed under a Creative Commons Attribution 4.0 International License, which permits use, sharing, adaptation, distribution and reproduction in any medium or format, as long as you give appropriate credit to the original author(s) and the source, provide a link to the Creative Commons licence, and indicate if changes were made. The images or other third party material in this article are included in the article's Creative Commons licence, unless indicated otherwise in a credit line to the material. If material is not included in the article's Creative Commons licence and your intended use is not permitted by statutory regulation or exceeds the permitted use, you will need to obtain permission directly from the copyright holder. To view a copy of this licence, visit <http://creativecommons.org/licenses/by/4.0/>. The Creative Commons Public Domain Dedication waiver (<http://creativecommons.org/publicdomain/zero/1.0/>) applies to the data made available in this article, unless otherwise stated in a credit line to the data.

Introduction

Small Cell Lung Cancer (SCLC) is a highly aggressive form of lung cancer accounting for ~15% of all lung cancer cases [1]. SCLC can be classified into molecular subtypes based on relative expression of the transcription factors including ASCL1 (SCLC-A), NEUROD1 (SCLC-N) and POU2F3 (SCLC-P) [2]. A more recent and broad classification considering both tumor intrinsic factors and immune-related genes has proposed an inflammatory subtype (SCLC-I) [3]. While generally considered a high-grade neuroendocrine cancer, SCLC tumors demonstrate a spectrum of neuroendocrine (NE) differentiation states [1]. The majority (~75%) of SCLC tumors, including those of the SCLC-A and -N subtypes, exhibit a high-NE profile [2, 4]. The rarer SCLC-P and SCLC-I typically define low- or non-NE subtypes [2, 3]. Although SCLC tumors can be generally characterized by a dominant subtype, analyses of both human SCLC and murine models of SCLC demonstrate substantial intratumoral cell state heterogeneity, and capacity for transformation between states [4–6]. Murine models of SCLC have demonstrated that *Ascl1*, a primary driver of the high-NE state, is a required factor in the development of SCLC [7]. Subsequent state plasticity with transition from high- to low-NE or mixed states has been associated with aspects of disease progression, including metastasis and acquired resistance to cytotoxic therapies [1].

State transitions in SCLC appear to be epigenetically determined rather than mutationally defined: no consistent genomic alterations differentiate these subtypes [2]. Some factors have been implicated as regulating high- to low-NE state transition in SCLC. Tumor progression and metastasis in a genetically engineered mouse model with a mutant *c-Myc* allele, was associated with transition from SCLC-A to SCLC-N subtype and in a subset of tumors to low-NE *Yap1*+SCLC [6, 8]. The role of *YAP1* as a subtype-defining factor in SCLC has been questioned by us and others [3, 4], including a report demonstrating that some long-established *YAP1*-expressing human SCLC cell lines might in fact be misattributed *SMARCA4*-deficient undifferentiated tumors [9]. Suppression of NOTCH signaling in a SCLC-A model has been shown to be essential for maintenance of the high-NE state [10], reflecting a similar role for NOTCH in inhibiting NE cell differentiation in fetal lung development [11]. Induction of NOTCH signaling in SCLC-A can promote SCLC state shift through at least two complementary mechanisms: [1] suppression of *ASCL1* and *ASCL1* target gene expression, and [2] upregulation of *REST*, a transcription factor that inhibits transcription of a set of NE genes including many non-overlapping from those under *ASCL1* control [12]. Inhibition of *ASCL1* and activation of *REST* appear to be required for full

transition to low-NE SCLC. Notably, the epigenetic regulators involved in SCLC subtype switching have not been fully defined. Pharmacologically tractable targets to constrain subtype plasticity in SCLC could have substantial clinical utility.

Mammalian SWI/SNF (BAF) ATP-dependent chromatin remodeling complexes are encoded by 29 genes, some of which are commonly mutated in cancer [13]. These complexes are classified into canonical BAF (cBAF), polybromo-associated BAF (PBAF) and noncanonical BAF (ncBAF). All SWI/SNF complexes contain *SMARCA2* or *SMARCA4* as an ATPase catalytic subunit that drives nucleosome sliding and eviction [14]. *SMARCA2* and *SMARCA4* demonstrate high homology, and *SMARCA2* upregulation can compensate for *SMARCA4* loss in some contexts [13]. SWI/SNF complexes modulate promoter and enhancer accessibility and have been shown to control multiple transcription programs including those related to cell and lineage differentiation. BAF complex members have divergent roles depending on the cancer context. As an example, *SMARCA4* loss accelerates tumor progression and promotes lung adenocarcinoma (LUAD) dedifferentiation [15], while abrogation of another key SWI/SNF component, *Arid1a*, suppresses tumor initiation and metastasis in hepatocellular carcinoma [16]. As a transcription factor (TF) implicated in multiple solid and hematologic malignancies, *SMARCA4* has recently gained attention as a therapeutic target [17–19]. The observation that *SMARCA2* can partially compensate for *SMARCA4* loss, and that these two homologous TFs are essential for activity of the SWI/SNF complexes, has led to the development of dual *SMARCA2/4* inhibitors [20, 21].

Loss of function mutations in *SMARCA4* are uncommon in SCLC (1.5%) but are substantially enriched in the non-NE SCLC tumors [22]. Consistently, *SMARCA4* mRNA levels are higher in NE SCLC (SCLC-A and -N) and in *POU2F3* cell lines than in either *YAP1*+SCLC or NSCLC [9]. These observations, together with data pointing to a role for the SWI/SNF complex in lineage differentiation [15, 23], prompted us to study the link between *SMARCA4* and subtype plasticity in the high- to low-NE transition in SCLC. Here, we provide evidence for a role of *SMARCA4* as a key regulator of the NE phenotype in SCLC, and as a potential target for the treatment of SCLC.

Material and methods

Animal models

Patient derived xenografts (PDXs) were subcutaneously engrafted into female 6-week-old NOD.Cg-Prkdc<scid>Il2rg<tm1Wjl>/SzJ (NSG) mice (5–10 mice per arm, Jackson Labs) whereas RP cells (3.5

million) were injected in one flank of female 8-week-old B6129SF1/J mice (Jackson Labs). Cells were resuspended in a mix of PBS and Matrigel 1:1 prior to injection. When tumors reached 75–100 mm³, mice were randomized and treated with either vehicle, FHD-286 (1.5 mg/kg twice daily dosing (BID) p.o.) or afatinib (15 mg/kg once daily dosing (QD) p.o.). Vehicle for FHD-286 consisted of 20% HP- β -CD in water whereas afatinib was dissolved in 0.5% methylcellulose in water. Tumors were measured twice per week with a caliper. Tumor volume was calculated as $((\text{width})^2 \times \text{length})/2$. All in vivo experiments were performed at Memorial Sloan Kettering Cancer Center (MSKCC) following Animal Care and Use Committee guidelines.

Cell lines

H82, H146, H69, H524, HCC33, SHP77, DMS114, H196, CORL311 and H211 were purchased from ATCC except for RP, which was a gift from Sage lab (Stanford), and culture in RPMI 1640 Medium (Gibco) supplemented with 10% tetracycline negative FBS (GeminiBio) and 1% Penicillin–Streptomycin (P/S). 293 T cells were also obtained from ATCC and cultured in DMEM media (Gibco), 10% FBS and 1% P/S. Cells were routinely tested for mycoplasma using the Universal Mycoplasma Detection Kit (ATCC). SMARCA4 and SMARCA2 genetic inhibition was induced by treating the cells with 1 $\mu\text{g}/\text{mL}$ at the indicated times for each experiment and renew every 48 h.

Cell proliferation assays and apoptosis

For cell proliferation assays, 2000 cells/well were seeded in 96 well-plates and treated with FHD-286 (5–1000 nM, Foghorn) and/or afatinib (10–150 nM, MedChem Express) for 96 h. Cell viability was determined by using CellTiter-Glo 2.0 Assay (Promega, G9242) following the manufacturer's instructions. Proliferation was determined by measuring the luminescence (L) at day 0, day 4 without drug and day 4 with drug. Proliferation was calculated by the ratio of L at day 4 with drug minus L at day 0 to the L without drug at day 4 minus L at day 0. In the case of the proliferation assays with genetic knock-downs, proliferation was calculated similarly by normalizing the L of each clone at the end of the experiment minus L at day 0 relative to the L of NTC cells at the end of the experiment minus L at day 0. IC_{50} was calculated with GraphPad Prism software whereas synergy scores were determined with SynergyFinder web application and using the ZIP method.

For apoptosis experiments, cells were seeded in 6 well plates and treated with FHD-286 (100 nM) and/or afatinib (500 nM) for 5 days. Then, cells were stained with FITC Annexin V and propidium iodide (PI) as indicated

by manufacturer (BD Pharmingen™ FITC Annexin V Apoptosis Detection Kit). Cell death was assessed by flow cytometry using a LSRFortessa™ Cell Analyzer.

Cell proliferation and apoptosis assays were performed at short intervals following treatment to explore the direct cytotoxic effects of FHD-286 in combination with afatinib.

Plasmid vectors, lentiviral virus production and transductions

To generate SMARCA4 and SMARCA2 knockdown (KD) cell lines, targeting shRNAs were cloned into the vector Tet-on LT3GEPiR (Addgene, #111177) with distinct antibiotic resistance, puromycin for SMARCA4 KD and neomycin for SMARCA2 KD. A non-targeting shRNA vector was used as control (NTC).

Lentiviral particles were produced by transfecting HEK293T cells (ATCC, no. CRL-1573) with the vector on interest in the presence of pMD2.G (Addgene #12259) and psPAX2 (Addgene #12260) packaging vectors (3:2:1 ratio of plasmid of interest: psPAX2:pMD2.G) and with JetPrime transfection reagent (Polyplus) as previously described [24]. Virus was collected after 72 h from transfection and concentrated 1:20 with Lenti-X™ Concentrator following manufacture's protocol (Takara Bio). Then, isogenic cell lines were spin-transduced (30' at 800G) with lentiviral particles and selected with the corresponding antibiotic. Doxycycline SMARCA4 and SMARCA2 inducible genetic inhibition was achieved by adding 1 $\mu\text{g}/\text{mL}$ of doxycycline every 48 h. All shRNAs and sgRNAs' sequences are detailed in Sup. Material Table.

Immunohistochemistry

Immunohistochemistry technique was performed as previously described [24]. FFPE slides from NE SCLC PDXs were first deparaffinized and steamed for 45 min in Target Retrieval Solution (Dako). Incubation with primary antibodies anti-NEUROD1 (Abcam, EPR 17084), anti-ASCL1 (BD, 24B72D11.11) and anti-SMARCA4 (Santa Cruz, sc-17796) was carried out following manufacturer instructions. Then, slides were incubated with PV PolyHRP anti-mouse IgG (Leica Microsystems, #PV6114) followed by a TSA biotin amplification step (Perkin Elmer) with DAB. Finally, slides were counterstained with hematoxylin and scanned on a Ventana DP 200 Slide Scanner (Roche).

Western blotting and PCR

For western blotting, cell pellets were lysed with cold RIPA buffer (Thermo Scientific) and incubated on ice for 30' followed by a centrifugation at 13,000 rpm at 4 °C for 30'. Protein quantification was performed using Pierce™

BCA Protein Assay Kit (Thermo Scientific). Antibodies used are detailed in Sup. Material Table.

RNA was isolated with the RNeasy Plus Mini Kit (Qiagen) following manufacturer's instructions and quantified using the NanoDrop ND-2000 spectrophotometer (Thermo Scientific). Then, 250 ng of RNA was retro-transcribed using qScript cDNA SuperMix (Quantabio). PCR reactions were carried out with 50 ng of cDNA using OneTaq Hot Start Quick-Load 2X Master Mix with Standard Buffer (New England Bio Labs), with cycling conditions of 30 s at 94°C; 40 cycles of 30 s at 94°C, 30 s at 55°C and 30 s at 68°C; and 5 min at 68°C. The amplified products were analyzed in a 2% agarose gel stained with GelRed Nucleic Acid Stain (MilliporeSigma).

Relative gene expression of REST4 variants was determined by RT-qPCR using SYBR TM Green PCR Master mix (Life Technologies) in a Gene Amp PCR System 9700 (Applied Biosystems). All primers used are detailed in Sup. Material Table.

Publicly available datasets (RNAseq, ChIP-seq and scRNAseq)

RNA levels of SMARCA4, SMARCA2, NE and non-NE markers in SCLC patients' tumors were assessed using George et al. [25] and Rudin et al. [26] databases. RNA expression levels in cell lines were retrieved from Cancer Cell Line Encyclopedia (CCLE, (<https://xenabrowser.net/>)). Expression levels were downloaded as RPKM (reads per kilobase of transcript per million reads mapped) and represented as RPKM or log (RPKM). SMARCA4 mRNA levels in LUAD and SCLC tumors were obtained from a cohort previously published by Quintanal Villalonga et al. [27] and express as log transformation of Transcripts per million (TPM). ASCL1 and NEURD1 ChIP-seq datasets were obtained from Borromeo et al. (GSE69394) [7]. The NE score was calculated using Zhang et al. signature [28]. We defined as high NE score when its value was >0 and low negative score when the value was <0.

Single cell RNAseq data from SCLC GEMM tumors was previously described and published by Ireland et al. [6]. Processed monocle2 cellular trajectory prediction object from Ireland et al. with normalized expression values, pseudotime projections and NE scores based on Zhang et al. [28] signatures were kindly provided by Dr. Trudy Oliver. Using the normalized expression values of RPM1-4 a Seurat object was created, data was scaled using *ScaleData* function, dimensionality reduction was applied using *RunPCA*, cellular neighbors were found by *FindNeighbors* function using the first 20 PCA and clusters were identified by Louvain approach (*FindClusters*, resolution=0.5) [29]. 2D embedding was performed using tSNE approach (*RunTSNE*, dim=20) and cellular

clusters were plotted. Using these embedded coordinates, SMARCA4 log transformed values as well as NE scores were plotted for each RPM cells. Similarly, log expression values for SMARCA4 and SMARCA2 (or any other gene), as well as NE scores for each cell were plotted using previously computed pseudotime profiles by Ireland et al. Code related to this analysis can be found at https://github.com/abcwcm/redin_smarca4.

ATAC-seq

H82 and H146 cells were treated with 100 nM of FHD-286 for 14 days and cryopreserved in cell freezing media (untreated and treated cells) until use. ATAC-seq sample preparation and sequencing was performed at Genewiz. Analysis was performed as previously published [24]. Raw sequencing reads were trimmed with Trim Galore (v0.4.4) (<https://github.com/FelixKrueger/TrimGalore>) for quality and Illumina adaptor sequences using the pair-end mode. Reads were then aligned to human assembly hg38 using bowtie2 v2.3.4 with the default settings [30]. Picard tool was used to remove reads with same start site and orientation. Enriched open regions for each sample were called using MACS2 and filtered against genomic blacklisted regions (<http://mitra.stanford.edu/kundaje/akundaje/release/blacklists/hg38-human/hg38.blacklist.bed.gz>) [31]. A union of Peak atlas was later built by merging the filtered peaks within 500 base pairs. Raw read counts were tabulated over this peak atlas using feature Counts v1.6.0 [32]. Differential peaks were called using DESeq2 [33]. For H146, three control samples were sequenced in one batch while one other control and three treated samples were sequenced in the second batch. The batch effect was counted as a co-variant with treatment using the multivariate model in DESeq2 to differentiate open regions in H146. The bigwig format for each sample was created using the BEDTools suite (<https://bedtools.readthedocs.io>) with the normalization factor from DESeq2 [33]. All bigwig genome tracks on interested gene regions were generated in Integrative Genomics Viewer (IGV) [34]. Replicates were collapsed using bigWigMerge, bedSort and bedGraphToBigWig form UCSC utilities binary tools to merge, sort and convert to bigwig format. The heatmap around significant differential regions with FDR <=0.01 and FC >=1.5 for each treatment in the format of collapsed bigwig was visualized using deeptools v3.4.0 [35]. Enriched motifs were identified from differential regions using HOMER v4.7 with mostly default settings [36]. The motifs were scanned in the differential peak regions as size given, controlled against all peaks as background.

Primary targets were identified as those DEG detected at RNAseq with a concordant change in chromatin

accessibility nearby (± 10 kb) the TSS. Predicted enhancers shown in Fig. 5F were identified using GeneHancer [37].

ChIP-seq

Chromatin immunoprecipitation sequencing (ChIP-seq) was performed at Active Motif (Carlsbad, CA, USA) using a monoclonal antibody against human SMARCA4 (#ab110641, Abcam). Validation of ChIP was assessed by qPCR before sequencing. A pool of the four PDXs was used as an input control. ChIP-Seq libraries were generated from the ChIP-DNA using a custom Illumina library type on an automated system (Apollo 342, Wafergen Biosystems/Takara). ChIP-Seq libraries were sequenced on Illumina NovaSeq 6000 as 75-nt single end reads. Adapter sequences were not trimmed during demultiplexing. Raw reads were processed using the same pipeline described in the ATAC-seq section. Enriched binding regions were called against the input using MACS2 [31] with p value < 0.001 . The bigwig format for each sample was created using the BEDTools suite (<https://bedtools.readthedocs.io>) with the normalization factor 10 million. ChIP density profiles were created with deeptools v3.4.0 [35]. Enrichment pathway analysis of ChIP-seq data was performed using the public web server ChIP-Enrich (<http://chip-enrich.med.umich.edu>). We used the method Poly-Enrich and the peaks were assigned to the nearest TSS [38, 39]. Motif enrichment analysis on the called peaks was performed using HOMER v4.7 [36]. ChIP-seq data was visualized with the Integrative Genomics Viewer (IGV) [34]. Promoter regions were defined as those within 5 kb from TSS whereas the proximal promoter region was named to the region within 1 kb from TSS.

RNA-seq

RNA isolation and sequencing was performed at Genewiz. RNA integrity and quantity was assessed with Qubit assay. Library preparation and sequencing was conducted with an Illumina sequencer. Fastq files were mapped to the human genome (hg38) and reads counts per gene were quantified using STAR [40] with default parameters and genecode (v28) annotation file. DEGs were identified with DESeq2 [33]. Combination of RNAseq data and public ASCL1 and NEUROD1 ChIP-seq was performed by integrating those genes downregulated at mRNA level upon treatment with FHD-286 ($p < 0.1$) with previously published ASCL1 and NEUROD1 targets [7]. Integration of RNAseq data with SMARCA4 ChIP-seq data was performed by combining genes downregulated by FHD-286 treatment ($p < 0.05$) with SMARCA4 binding gene promoters (< 5 kb) detected in at least 2 out of 4 PDXs in the ChIP-seq data.

Pathway enrichment analysis by GSEA, ENRICH and Ingenuity

Gene set enrichment analysis (GSEA, v4.0.2) [41] was conducted using ClusterProfiler R package v3.18 [42]. Analysis was performed on the full set of genes ranked by p value scores computed as $-\log(p \text{ value}) \times (\text{sign of } \log_2\text{FC})$ from differential expression analyses between FHD-286 treated cells and parental cells. Gene set annotations were obtained from Molecular Signatures Database (MSigDB v7.0.1 [41, 43]) and the enrichment was calculated by using permutation test with p value adjustment by Benjamin-Hochberg procedure. NE and non-NE gene sets consist of a 25 genes list each from Zhang et al. signature [28]. Normalized enrichment scores (NES) and q or p values are detailed in the figure legends.

ENRICH analysis [44, 45] was applied to all genes significantly ($p < 0.05$) downregulated between treated and untreated cells in both H82 and H146 cell lines detected at RNAseq as detailed in Figure S7F. ENRICH analysis was performed to those confident targets identified by combining downregulated DEGs (RNAseq) with SMARCA4 targets binding to promoter regions in at least 2 out of 4 PDXs assessed (Fig. S6A). Pathway enrichment analysis with ENRICH was also applied to all genes with a significant ($p < 0.05$) downregulation in the accessibility detected at any genomic region in both cell lines (Fig. S4E).

To characterize pathways enriched or inhibited after inhibition of SMARCA4 we conducted Ingenuity Pathway Analysis (IPA, Qiagen, <https://www.qiagenbioinformatics.com/products/ingenuity-pathway-analysis>) on only differential ($p < 0.01$) upregulated or downregulated genes between FHD-286 treated vs untreated cells detected at RNA-seq data. Data was presented by plotting the Z score, which is calculated based on the data set's correlation with an activated state and the log transformation of the p value.

Statistical analysis

Statistical comparison between two groups was performed applying unpaired two-tailed Student's t test (parametric). For multiple comparisons, one- or two-way ANOVA analysis followed by Bonferroni post-hoc test was used. For correlation analysis, Spearman analysis was used. Fisher analysis was performed to explore the association between the NE score (< 0 or > 0) and expression of SMARCA4 (< 0 or > 0). Data was analyzed with GraphPad Prism 9 software and statistical significance was defined as $p < 0.05$ (*), $p < 0.01$ (**), $p < 0.001$ (***), $p < 0.0001$ (****). The analysis used is detailed in the figure legend of each experiment. All functional experiments were replicated a minimum of three times. All western

blots were reproduced a minimum of two times with independent protein extracts from biological replicates for a given model, and in a minimum of two different models to support universality of the findings.

Results

SMARCA4 is highly expressed in neuroendocrine SCLC

We first sought to evaluate relative expression levels of *SMARCA4* across the spectrum of human cancers. *SMARCA4* expression was higher in SCLC lines than in any other solid tumor represented in the Cancer Cell Line Encyclopedia (CCLE) (Fig. 1A). Focusing on lung cancer biopsy specimens, *SMARCA4* levels were also significantly higher in SCLC than in lung adenocarcinoma (Fig. 1B). Up to 75% of all SCLC tumors are classified as NE-high, based on upregulated expression of *ASCL1* and/or *NEUROD1* and a variety of NE markers. *SMARCA4* expression was positively correlated with multiple NE genes including *SYP*, *CHGA*, *INSM1*, *DLL3* and *NCAM1* and negatively correlated with non-NE factors *REST*, *NOTCH2*, and *YAP1* in both SCLC cell lines and patient tumor databases (Figs. 1C and S1A). Stratification of SCLC tumors and cell lines based on the expression of an NE score determined by applying Zhang et al. signature [28] showed significantly lower *SMARCA4* expression in low-NE versus high-NE SCLC samples (Fig. 1D).

SMARCA4 expression might be a secondary effect of a NE-high state or might be a factor driving the NE phenotype. To assess whether SWI/SNF activity might promote the expression of NE factors in SCLC, we genetically downregulated the expression of *SMARCA4* and/or *SMARCA2* using a Tet-On inducible shRNA system. Genetic inhibition of *SMARCA4* led to compensatory upregulation of *SMARCA2* expression, as previously described [13, 46] (Fig. S1B). Single inhibition of *SMARCA2* did not change the protein expression of the master regulators *NEUROD1* and *ASCL1*, or of the NE factors *SYP* or *CHGA*, in H82 (SCLC-N) or H146 (SCLC-A). *SMARCA4* knockdown slightly reduced some of these markers, and dual inhibition of *SMARCA4* and *SMARCA2* markedly decreased NE factor expression (Fig. 1E). Single knockdown of each gene did not affect cell proliferation while double knockdown of *SMARCA2/4* significantly reduced the proliferative capacity of the cells in vitro (Fig. S1C).

Pharmacological inhibition of SMARCA2/4 with FHD-286 downregulates neuroendocrine and neuronal signaling pathways

To explore the potential role of *SMARCA4* as a regulator of NE cell fate, we used the dual allosteric *SMARCA2/SMARCA4* ATPase inhibitor FHD-286 (Foghorn

Therapeutics), a small molecule, orally bioavailable, BRG1 and BRM-selective, ATPase inhibitor. Based on its potent pre-clinical activity against cancer cells including leukemia and lung adenocarcinoma cells, FHD286 is currently being evaluated for safety and clinical efficacy in early clinical trials in AML (NCT04891757) [20, 21]. We characterized gene expression changes in H82 (SCLC-N) and H146 (SCLC-A) cells upon treatment with FHD-286 by RNAseq (Figs. 2A and S2A, B). Pharmacological inhibition of *SMARCA4* induced downregulation of many key NE factors, and upregulation of factors associated to the low-NE phenotype, including *REST* (Figs. 2A and S2C, D and Table S1). Gene set enrichment analysis (GSEA) of differentially expressed genes (DEG) revealed downregulation of neuronal and NE pathways in both H82 and H146 cells treated with FHD-286, including decrease in *ASCL1* targets in the SCLC-A line H146 (Fig. 2B). Ingenuity pathway enrichment analysis of reduced expressed genes ($p < 0.01$) confirmed the downregulation of neuronal related pathways (Fig. S2E). GSEA leveraging publicly available high- and low-NE signatures derived from SCLC cell lines [28] supported a shift from a high- to a low-NE phenotypic state (Fig. 2C). Accordingly, upon inhibition of *SMARCA4* we observed not only a reduction of *ASCL1* and *NEUROD1* TFs but also of their most confident targets previously identified by Borromeo et al. [7] (Fig. 2D). Consistent with this high- to low-NE transition, we detected a significant gain in the expression of multiple Hippo signaling targets (*YAP1*, *TEAD2*, *AJUBA*, *CYR61*, *WWTR1*) and NOTCH targets (*HES1* and *HEY1*) upon treatment in both models (Fig. 2E, F). GSEA confirmed the activation of Hippo and NOTCH signaling in H82 cell line upon FHD-286 treatment with similar trends observed in H146 (Fig. S2F). We validated the downregulation of the NE markers *NEUROD1*, *ASCL1* and *SYP*, and increase of *NOTCH2* and *HES1*, both involved in promoting low-NE differentiation in SCLC [10, 12], at the protein level after treatment with FHD-286 (Fig. 2G). Reduction in the expression of NE markers along with increase of *NOTCH2*, *HES1* or *YAP1* was also confirmed at the protein level after dual genetic inhibition of *SMARCA4/2* (Fig. S2G).

To study the association of *SMARCA4* and NE identity in SCLC at higher resolution, we leveraged a publicly available scRNAseq dataset of 4 tumors derived from the *Rb1^{fl/fl}; Trp53^{fl/fl}; MycT58A^{LSL/LSL}* (RPM) genetically engineered mouse model (GEMM) of SCLC [6]. In this GEMM, *c-Myc* promotes tumor transition from a high-NE state into a low-NE state (Fig. S3A). Each cell was assigned with a NE score by applying a previously defined NE gene signature [28] (Fig. 2H). Cells with high *SMARCA4* mRNA levels corresponded to those exhibiting a high NE score, whereas low NE cells lacked

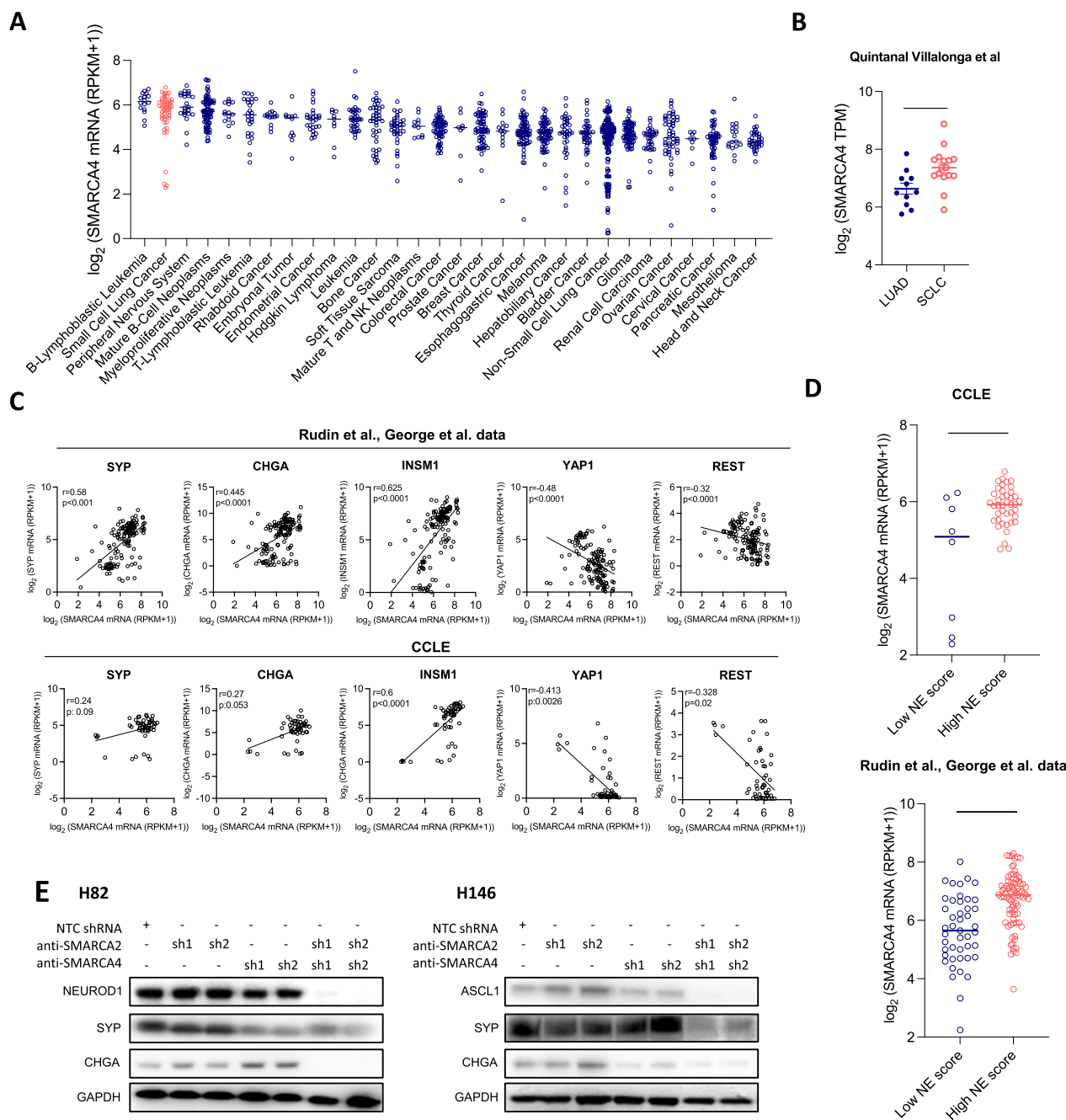


Fig. 1 SMARCA4 expression correlates with NE features in SCLC. **A** SMARCA4 mRNA levels in cell lines derived from 30 tumor types assessed using the Cancer Cell Line Encyclopedia (CCLE). Bars indicate the median expression per tumor type. **B** SMARCA4 mRNA levels in LUAD and SCLC specimens retrieved from Quintanal Villalonga et al. [27]. Student's two-tailed unpaired t test. $**p < 0.01$. **C** Spearman correlation of SYP, CHGA, INSM1, YAP1 and REST with SMARCA4 mRNA levels in Rudin et al. and George et al. databases and CCLE [25, 26]. **D** SMARCA4 mRNA expression in low and high NE SCLC tumors in cell lines (CCLE) and clinical specimens (Rudin et al. and George et al.) [25, 26]. One-way ANOVA test followed by Bonferroni post-hoc test. $****p < 0.0001$, $***p < 0.001$, $**p < 0.01$. **E** Western blotting of ASCL1, NEUROD1, SYP and CHGA in isogenic cell lines derived from H82 and H146 expressing different combinations of shRNAs against SMARCA4 and/or SMARCA2. Expression of shRNAs from **E** was conditional of doxycycline treatment. Protein collection and blotting was performed after 14 days of doxycycline treatment. See also Fig. S1

SMARCA4 expression (Figs. 2H, S3B and Table S1). Fisher analysis applied to these data confirmed the significant association between the presence of *SMARCA4* and a high NE score (Fig. S3B). We also analyzed *SMARCA4* expression changes in an unsupervised pseudotime trajectory constructed by Ireland et al. [6]. Cells belonging to early pseudotime showed high NE score and high *SMARCA4* while in late pseudotime progression, cells had reduced NE score and reduced *SMARCA4* (Figs. 2I and S3C, D). No changes in *SMARCA2* levels were found along the pseudotime trajectory (Fig. S3D). Taken together, these data suggest that *SMARCA4* is required for SCLC cells to maintain high NE identity.

SMARCA4 inactivation alters chromatin accessibility in neuroendocrine SCLC

We next explored whether *SMARCA4* could control the chromatin accessibility of NE and non-NE genes as mechanism of regulating their mRNA expression. Suppression of *SMARCA4* activity by FHD-286 induced global changes in the accessibility with a predominance in the number of lost regions: > 35,000 sites lost in both H82 and H146 cells (Figs. 3A and S4A–C). Notably, reduced accessible genomic regions upon FHD-286 had a striking enrichment for the DNA-binding proneuronal and NE genes motifs *ASCL1*, *NEUROD1*, *OLIG2*, *ATOH1*, *NEUROG2*, *FOXA2*, *FOXA1* and *OTX2* (Figs. 3B and S4D). *OTX2* is selectively expressed in *NEUROD1*^{high} SCLC cells, and its DNA motif is also enriched at *NEUROD1*-bound sequences [7]. Changes in gene loci accessibility were mainly located at TSS distal regions (< 10 kb from TSS), as observed in other tumors such as lung adenocarcinoma [20] (Fig. 3C and Table S2). Among the genes with reduced distal accessibility changes we identified relevant NE genes, but we did not find evidence of increased accessibility in non-NE genes previously found upregulated at the mRNA level after FHD-286 treatment or reduced accessibility around the TSS of *ASCL1*, *NEUROD1*, *SYP* or *CHGA* among others (Fig. 3C, D). Pathway enrichment analysis of genes with sites of

lost accessibility ($p < 0.05$) in both cell lines ($n = 6666$), revealed a strong enrichment in neuronal pathways, supporting a role for *SMARCA4* in regulating chromatin accessibility of NE genes (Figs. 3E and S4E). Lastly, we integrated the differential ATAC-seq peaks within 10 kb up or downstream of gene TSS with our RNAseq data to identify *SMARCA4* primary targets. In line with our previous findings, only 12.5% (H82) and 21.4% (H146) of genes downregulated, and 20.6% (H82) and 26.6% (H146) or genes upregulated, showed a concordant change in accessibility around the promoter region (± 10 kb) (Table S2).

SMARCA4 binds to neuronal and NE lineage TF genes in SCLC

To better understand how the *SMARCA4*-containing SWI/SNF complex controls NE cell fate in SCLC, we performed ChIP-seq of *SMARCA4* in four NE SCLC patient-derived xenografts (PDXs) with high levels of *SMARCA4* (Fig. S5A) and no mutations in any of the SWI/SNF complex subunits (Fig. S5B). *SMARCA4* binding peaks were detected in promoter regions (within 5 kb upstream of TSS), 5'UTR, exons, introns and 3'UTR (Figs. 4A and S5C). Peak annotation identified 20,754 (Lx95), 17,994 (Lx276), 16,556 (Lx761c) and 15,655 (Lx891) *SMARCA4* candidate gene targets. *SMARCA4*-bound promoters included those of the lineage-specifying TFs *ASCL1* and *NEUROD1* and many other NE genes (*SYP*, *CHGA*, *INSM1*, *FOXA2*, *DLL3*, *GRP*, *FOXA1*) (Figs. 4B, C and S5D). Interestingly, *SMARCA4* binding to *ASCL1* was not only detected at the TSS (as is also the case for *NEUROD1*) but at sites along the entire *ASCL1* gene body (Fig. 4B). We next explored whether the downregulation of *ASCL1* and *NEUROD1* top confident targets, observed following *SMARCA4* inhibition (Fig. 2D), could be a consequence of *SMARCA4* direct binding [7]. Consistent with this hypothesis, 96% of *ASCL1* targets and 80% of *NEUROD1* targets were detected as *SMARCA4*-bound genes in at least 3 out of 4 PDXs analyzed, suggesting that *SMARCA4* binding might be required to

(See figure on next page.)

Fig. 2 *SMARCA4* inhibition suppresses the NE phenotype in SCLC. **A** Hockey-stick plots of DEGs in FHD-286-treated cells after 14 days (100 nM) versus control, untreated cells. (See Table S1). **B** Dot plots showing negative enrichment in selected neuronal and NE pathways analyzed by GSEA in RNAseq data from H82 and H146 cell lines treated with FHD-286 versus untreated. (See Table S1). **C** GSEA applying Zhang et al. NE gene signature [28] in H82 cell line treated with FHD-286 versus untreated. **D** Heatmaps showing the most significant confident targets (top 25 with TPMs > 2) of *NEUROD1* (left) and *ASCL1* (right) [7], in H82 (left) and H146 (right) bulk RNAseq (FHD-286 treated vs untreated). **E** Log₂ fold change of Hippo pathway genes from data in A. Student's two-tailed unpaired t test. *** $p < 0.001$, ** $p < 0.01$. The mean \pm SD is shown. **F** Log₂ fold change of NOTCH pathway genes from data in A. Student's two-tailed unpaired t test. *** $p < 0.001$, * $p < 0.05$. The mean \pm SD is shown. **G** Western blotting of H524 (SCLC-N), H82 (SCLC-N), HCC33 (SCLC-N), H69 (SCLC-A), SHP77 (SCLC-A) and H146 (SCLC-A) cells after treatment with 100 nM of FHD-286 for 7 and 14 days. **H** t-SNE of Zhang NE signature and *SMARCA4* levels applied to public scRNAseq data of 4 myc-driven murine (RPM) tumors [6]. **I** Scoring for Zhang NE signature and *SMARCA4* projected in a pseudotime trajectory from early to late time points in a tumor from a Myc-driven murine SCLC model showing subtype plasticity [6]. See also Figs. S2, S3 and Table S1

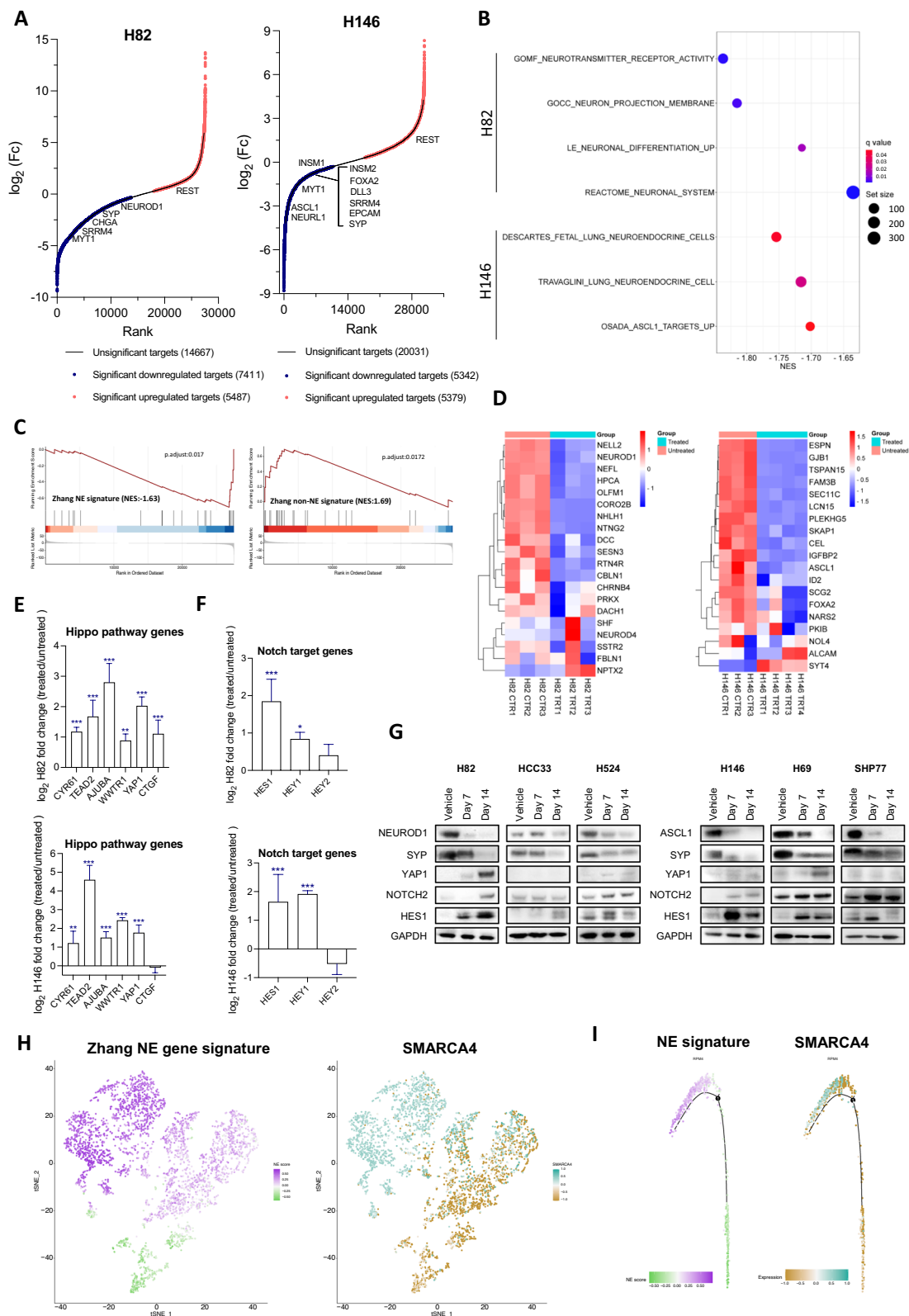


Fig. 2 (See legend on previous page.)

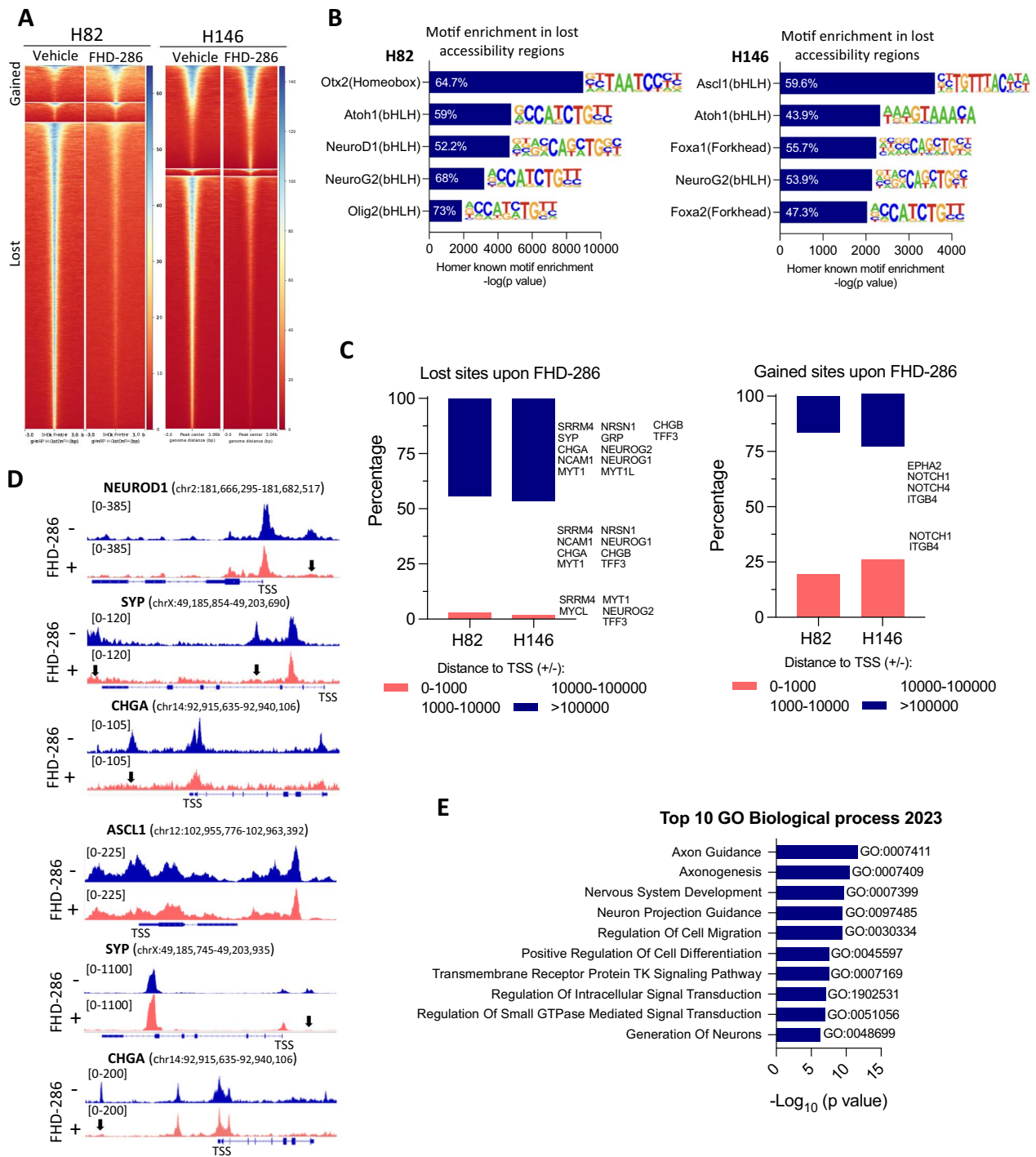


Fig. 3 SMARCA4 inactivation alters chromatin accessibility in NE-high SCLC. **A** Heatmap showing ATACseq chromatin accessibility changes (FDR:0.01, FC > 1.5) in H82 and H146 cells after treatment with FHD-286 (100 nM, 14 days). **B** Enrichment of neuronal and NE HOMER transcription factor-binding DNA motifs in ATAC-seq peaks lost after treatment with FHD-286 (100 nM, 14 days). The percentage indicates the amount of target sequences with motif. **C** Genomic localization of lost and gained accessible sites upon FHD-286 treatment in H82 and H146 cells. **D** ATACseq genome tracks of *NEUROD1*, *SYP* and *CHGA* in H82 and H146 cells after treatment with FHD-286. Peaks with a significant reduction in chromatin accessibility are indicated with arrows. **E** Enrich analysis applied to all genes with lost sites (across all gene body) following FHD-286 treatment. Top 10 GO Biological processes enriched are shown. See also Fig. S4

fully activate their transcription (Fig. S5E). Poly-Enrich analysis of SMARCA4 ChIP-seq binding profile predicted strong enrichment in neuron development and differentiation biological processes based on SMARCA4 targets (Fig. 4D). We also found enrichment in regulators of NOTCH signaling, including negative regulators of this pathway, and chromatin remodeling and organization processes (Fig. S5F).

We next cross-referenced SMARCA4 binding promoter regions (< 5 kb) identified by ChIP-seq with genes downregulated by FHD-286 treatment as determined by RNAseq to identify high-confidence SMARCA4 targets. This analysis nominated 617 common SMARCA4 targets in both ASCL1 and NEUROD1 SCLC subtypes (Fig. S6A and Table S3). Pathway enrichment analysis of these confident targets again showed neuron related processes among the top GO Biological processes regulated by SMARCA4 (Fig. 4E). With the aim of identifying which DNA-binding motifs are the most enriched within SMARCA4 ChIP-seq peaks we performed HOMER analysis. Remarkably, 52.7% of all motifs detected overlapped in at least 3 out of the 4 PDXs analyzed (Fig. S6B). We found a significant enrichment in known motifs of the neuronal and NE lineage TFs NEUROD1, ASCL1, FOXA2, ATOH1 and NEUROG2 (Figs. 4F and S6C). Remarkably, most of these motifs matched those with reduced accessibility after FHD-286 treatment and identified by ATACseq (Fig. 3B). A complete list of the gene motifs detected in the ChIP-seq data is found in Table S3.

SMARCA4 regulates common ASCL1 and NEUROD1 targets and induces REST splicing by SRRM4

We next sought to identify convergent downstream targets of ASCL1 and NEUROD1 under the control of SMARCA4, with a potential role in NE differentiation. Combining our RNAseq data (genes inhibited by FHD-286) and publicly available ChIP-seq data of ASCL1 and NEUROD1 we identified 8 common targets (Fig. 5A) [7]. Among these candidates, we selected Reticulon 1 (*RTNI*), Neurensin 1 (*NRSNI*), Myelin transcription factor (*MYT1*) and Serine/Arginine Repetitive Matrix (*SRRM4*), as promising targets of the SMARCA4/ASCL1/NEUROD1 axis because of their suggested roles in

sustaining the NE phenotype and neuronal development [47–50]. Western blotting revealed a strong inhibition of all four targets upon treatment with FHD-286 and after genetic inhibition of SMARCA4/2 (Figs. 5B and S7A). SMARCA4 ChIP-seq showed binding of SMARCA4 to the TSS of all four genes, defining them as high confidence targets of SMARCA4 (Figs. 5C and S7B). Analysis of *RTNI*, *NRSNI*, *MYT1* and *SRRM4* levels in scRNAseq pseudotime trajectory of the GEMM SCLC model demonstrating subtype plasticity (Fig. 2H, I) [6] also confirmed loss of expression of these four genes in the transition from high- to low-NE state in SCLC (Fig. S7C). Consistently, we observed a positive correlation of *SMARCA4* expression with that of all 4 genes in patients' SCLC samples (Figs. 5D and S7D). Additional correlation analysis between *SMARCA4* and *SRRM4* across the pan-cancer CCLE dataset revealed two well-defined groups: one including cell lines expressing *SMARCA4* and lacking *SRRM4*, and another group with a strong positive correlation between these genes. The cell lines belonging to the latter group were almost entirely comprised of tumor types with NE/neuronal features, suggesting that *SRRM4* expression may be restricted to NE tumors (Fig. 5E).

Given the activity of *SRRM4* in regulating RNA splicing of *REST*, a known transcriptional driver of low-NE cell fate in SCLC [12, 51], we decided to delve deeper into its role. Alternative splicing of *REST* by *SRRM4* induces the incorporation of the exon N3c into the transcript, leading to the expression of the truncated and non-functional derivative, *REST4*. Reduction of active *REST* by *SRRM4*-driven splicing has been shown to promote a NE phenotype in prostate tumors [50, 52, 53]. In addition to SMARCA4 binding to the *SRRM4* promoter, we found that pharmacological targeting of SMARCA2/4 significantly reduced DNA accessibility of *SRRM4* regulatory elements, including promoter (for H82) and enhancers regions (Figs. 5F, 3C). To investigate the role of SMARCA4 in *REST* splicing through *SRRM4*, we first analyzed the different splicing isoforms of *REST* harboring N3c exon (Fig. 5G). Inactive *REST4* variants (S3, S7 and S12) were consistently present in high-NE and undetectable in low-NE SCLC cell lines (Fig. S7E).

(See figure on next page.)

Fig. 4 SMARCA4 binds to neuronal and NE lineage TF genes in SCLC. **A** Heatmap and metaplot showing SMARCA4 binding profile determined by ChIP-seq in 4 NE SCLC PDXs and a pooled input. The range under the map indicates the ChIP-seq signal intensity. **B** Metaplots of *ASCL1* and *NEUROD1* in all PDXs and input. Heatmaps showing the binding of SMARCA4 to *ASCL1* and *NEUROD1* gene bodies. The range indicates the normalized enrichment along the respective gene regions. **C** NE lineage TFs and gene promoter proximal regions (within 1 kb of TSS) bound by SMARCA4 in NE SCLC PDXs. **D** Dot plot of Poly-Enrich analysis applied to SMARCA4 ChIP-seq peaks. Fold enrichment refers to the fold increase in the signal for a particular gene relative to the background signal. The counts refer to the number of genes detected in the ChIP-seq data that are part of the indicated pathways. **E** Enrich analysis of 617 consensus genes selected by combining RNAseq from Fig. 2 and ChIP-seq data. See also Fig. S5E. **F** Enrichment analysis of TF-binding motifs in the SMARCA4 ChIP-seq data identified with HOMER. See also Figs. S5, S6 and Table S3

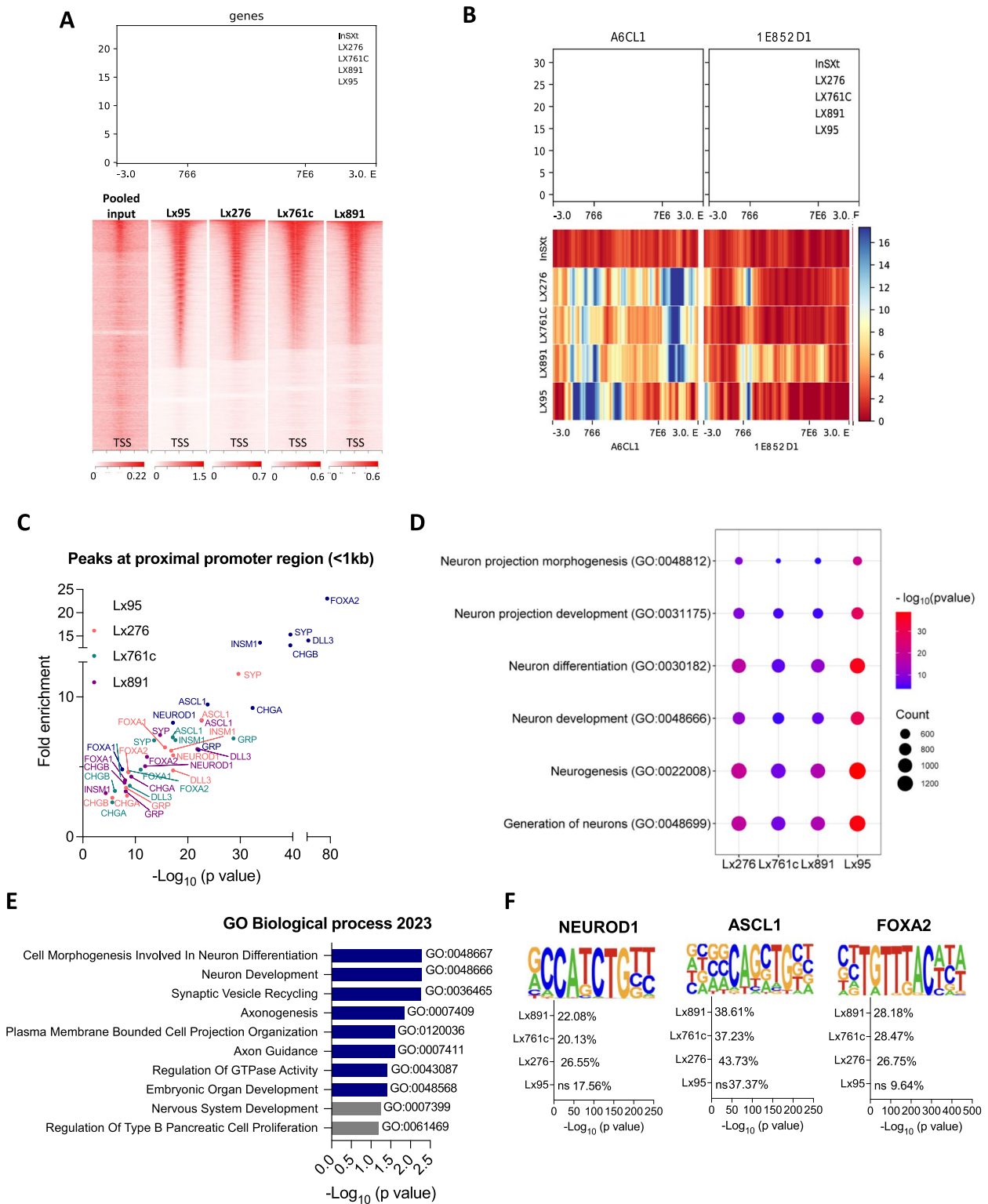


Fig. 4 (See legend on previous page.)

Pharmacological inhibition of SMARCA4 with FHD-286 increased the abundance of non-N3c active isoforms (S11/S16/S18) including the canonical one (S1) while reducing inactive *REST4* isoforms S3 and S12. The variant S7 did not change after treatment (Fig. 5H). To quantify the relative amount of *REST4* isoforms after treatment with FHD-286, we performed RT-qPCR using a pair of primers (E3N3c/E4R2) spanning N3c of all three *REST4* variants (Fig. 5I). Pharmacological inhibition of SMARCA4 strikingly reduced the relative levels of inactive *REST4* (S3, S7 and S12) in all NE cell lines tested (Fig. 5I). Consistent with these results, Enrichment analysis performed on those genes commonly and significantly downregulated at mRNA level ($n=904$; Fig. S7F) nominated REST as the top and only significant TF involved in the loss of NE markers after SMARCA4 inhibition (Fig. 5J). Taken together, these findings demonstrate that SMARCA4 controls *REST* splicing by sustaining the expression of SRRM4.

SMARCA4 suppression by FHD-286 activates ERBB pathways and sensitizes to afatinib

Finally, we evaluated the potential of SMARCA4 pharmacological inhibition as a therapeutic approach for SCLC tumors. Cell proliferation assays in vitro showed response to FHD-286 across a panel of SCLC lines, in the nanomolar range (median IC_{50} of 90 ± 45.9 nM), except for YAP1+SCLC low-NE lines, which showed IC_{50} values above 200 nM (Figs. 6A and S8A). In vivo treatment of two high-NE SCLC PDX models with single agent FHD-286 at a dose of 1.5 mg/kg twice daily demonstrated limited growth inhibition (Fig. 6B).

We sought to identify vulnerabilities induced by SMARCA4 inactivation. Ingenuity pathway analysis (IPA) of differential upregulated genes ($p < 0.01$) detected by RNAseq in treated vs untreated cells suggested activation of ERBB and Neuroregulin-1 (NRG1) pathways upon FHD-286 treatment (Fig. 6C). Consistently, FHD-286 treatment in two NE SCLC cell lines induced protein

upregulation of ERBB family receptors ERBB2, ERBB3 and ERBB4 (Fig. 6D), and of NRG1 (Figs. 6E and S8B), a direct ligand and activator of ERBB proteins. In line with ERBB pathway activation, we observed increased phosphorylation of the downstream targets ERK and AKT (Figs. 6E and S8B). Addition of recombinant NRG1 to the NE SCLC cell lines H82 and H146 supported a role of NRG1 as ligand and activator of ERBB pathway in SCLC, inducing phosphorylation of ERK and AKT (Fig. S8C). These results suggest that SMARCA4 inhibition might drive the activation of the NRG1-ERBB pathway in SCLC.

We therefore investigated whether the pharmacological blockade of ERBB pathway with the irreversible inhibitor afatinib could synergize with FHD-286. Drug combination assays demonstrated a strong synergy between these drugs in all 4 SCLC subtypes cell lines tested (hsa synergy score: 8–17.5) (Figs. 6F and S8D), accompanied by increased cell death relative to either single agent treatment (Fig. 6G). Accordingly, ectopic silencing of either SMARCA4 or SMARCA4/SMARCA2 increased the effectiveness of afatinib in vitro (Fig. S8E).

In the light of these results, we explored the combination of FHD-286 and afatinib in vivo in a set of chemoresistant SCLC PDXs and in an immunocompetent mouse model. Afatinib monotherapy did not reduce tumor growth in any of the models tested except for LX1042, a PDX derived from an *EGFR*-mutant adenocarcinoma that transformed to SCLC on targeted therapy (Fig. 6H). SMARCA4/2 inhibition with FHD-286 monotherapy slightly decreased tumor growth in all models tested; in contrast, the combination of FHD-286 with afatinib induced strong growth-suppressive responses in all models assessed (Figs. 6H and S8F).

Discussion

SCLC is the most lethal form of lung cancer, with limited therapeutic options. Transcriptional profiling has been used to classify SCLC into high-NE (ASCL1 and/

(See figure on next page.)

Fig. 5 SMARCA4 regulates SRRM4 expression to control splicing and activation of REST. **A** Venn diagram of ASCL1 and NEUROD1 published binding targets from Borromeo et al. [7] overlapping with genes downregulated by FHD-286 in H146 and H82 cells. **B** Western blots of H82 and H146 cells treated with FHD-286 for 14 days. **C** Metaplot of SMARCA4 ChIP-seq showing SMARCA4 binding to *SRRM4* in 4 NE SCLC PDXs. Range indicates the fold enrichment with respect to the input. ChIP-seq genome tracks at *SRRM4* TSS. Graphs were obtained from IGV. **D** Correlation of *SMARCA4* and *SRRM4* mRNA levels in SCLC patients' database. Spearman correlation. **E** Correlation analysis of *SRRM4* and *SMARCA4* in cancer cell lines retrieved from CCLE. Cell lines with both high *SMARCA4* and *SRRM4* mRNA levels are highlighted. **F** Merged ATAC-seq tracks of H82 and H146 parental cells and FHD-286 treated cells (day 14) at *SRRM4* gene locus visualized with IGV. **G** Graphical representation of REST genomic regions and spliced isoforms with the binding location of the different primers used for PCR. **H** PCR analysis of *REST* splicing isoforms using two pairs of primers (E2F1 + E4R1 and E1F1 + E4R1) that span N3c. **I** RT-qPCR of *REST4* isoforms (S3, S7, S12) in H82, H146 and H524 treated with FHD-286 (14 days) versus untreated cells. The pair of primers E3N3c and E4R2 that recognizes all isoforms including exon N3c was used. Student's two-tailed unpaired t test. *** $p < 0.001$. The mean \pm SD is shown. **J** Enrich analysis applied to commonly and significantly downregulated genes in both H146 and H82 ($n=904$) cell lines identified in the bulk-RNAseq (Fig. 2). See also Fig. S7

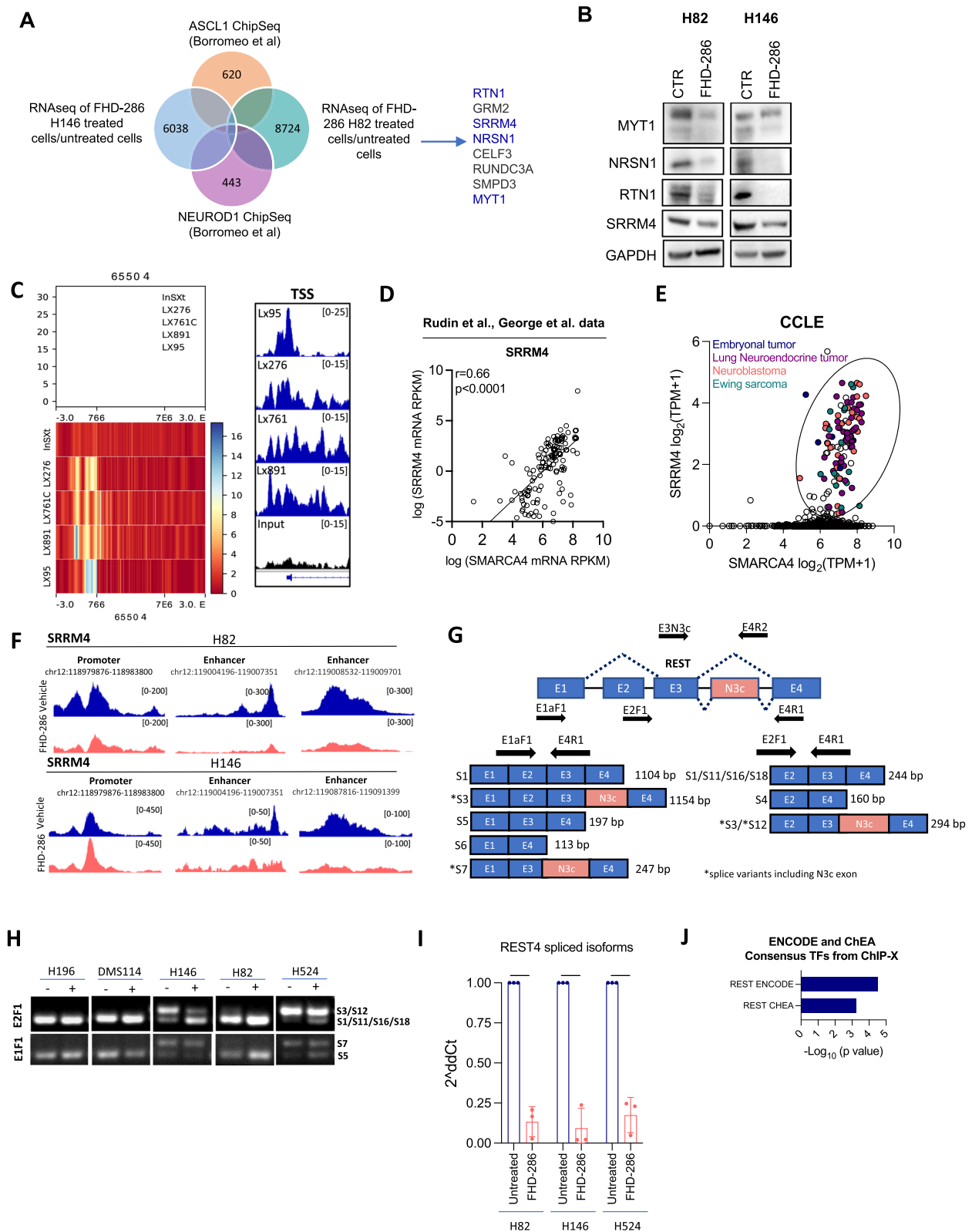


Fig. 5 (See legend on previous page.)

or NEUROD1+) and low-NE (POU2F3 and/or Inflamed) states [2, 3]. ASCL1 and NEUROD1 are well established transcription activators of NE genes, but it is unclear which factors enforce the maintenance of the NE-high state, or regulate cell state transitions between high- and low-NE phenotypes [7, 54–57]. Here, we report SMARCA4 as a critical regulator of the NE phenotype and as a therapeutic vulnerability in SCLC (Fig. 6I).

Coexistence of NE and non-NE cells in GEMM models was one of the first observations pointing to cell state plasticity in SCLC [58]. Activation of *c-Myc* can facilitate transition of SCLC-A tumors to SCLC-N and Yap1+SCLC in a GEMM [6]. Abrogation of epigenetic regulators including EZH2, LSD1 and KMD6A have been also associated to phenotypic switching between subtypes in SCLC [59–61]. Simultaneous detection of molecular subtypes, and shifts associated with disease progression, have been observed in human SCLC [6, 62]. Here we show that the chromatin remodeler SMARCA4 sustains the NE phenotype in both ASCL1 and NEUROD1 SCLC subtypes, and that its inactivation promotes a shift toward a low-NE state. In silico analysis showed a strong correlation between levels of SMARCA4 and NE markers in both SCLC patient tumors and cell lines. ChIP-seq of SMARCA4 in NE-high SCLC PDXs revealed binding to regulatory elements of lineage TFs including *ASCL1*, *NEUROD1*, *FOXA2* and *INSM1* as well as to relevant genes implicated in axonogenesis, synapse formation, and neuropeptide signaling pathways. Several genes identified as high-confidence SMARCA4 binding targets overlapped with ASCL1 and NEUROD1 targets, suggesting a role for SMARCA4 in regulating ASCL1 and NEUROD1 downstream transcriptional programs [63]. Accordingly, we found reduction in chromatin accessibility at distal regions across a spectrum of NE genes when SMARCA4 was pharmacologically inhibited. Phenotypic changes driven by SMARCA4 inactivation have been previously described in other tumors, including lung adenocarcinoma, where SMARCA4 has a cell-type specificity role in lineage transformation and exhibits divergent functions depending on the cell of origin [15]. mSWI/SNF complex has been recently reported as a

dependency in POU2F3 SCLC tumors [64, 65]. Intriguingly, SMARCA4/2 inhibition affects distinct programs in POU2F3 SCLC cells than those we have observed in SCLC-A and SCLC-N, suggesting a different function for SMARCA4 in high vs low-NE SCLC subtypes.

Notably, SMARCA4 binds to several known regulators of NOTCH signaling. Activation of NOTCH has been shown to promote non-NE fate by increasing REST and HES1 in SCLC [12, 66]. Whether SMARCA4 functions as a transcriptional repressor of some of these NOTCH regulators in SCLC is still unknown and requires further investigation. REST is a key regulator of non-NE differentiation, and its activation appears necessary to achieve transition to a non-NE state in SCLC [12, 67, 68]. REST has been shown to be spliced to encode the inactive REST isoform REST4 by SRRM4 in NE prostate and SCLC tumors [50, 52, 53, 69, 70]. However, upstream molecular mechanisms underlying SRRM4 activation in NE tumors had not been defined. We confirmed REST splicing into inactive REST4 variants in NE-high SCLC and demonstrated that SMARCA4 inhibition with FHD-286 reduced the levels of inactive REST4 through downregulation of SRRM4. SMARCA4 binds to the *SRRM4* promoter and its inhibition reduces the chromatin accessibility of SRRM4. Enrichment analysis of DEG identified REST as the top TF associated with SMARCA4 driven non-NE SCLC transition. Interestingly, a recent study has shown that REST and ASCL1 regulate distinct cell fate targets in SCLC and suggested that inhibition of ASCL1 and activation of REST are both required to promote a NE to non-NE transition [12]. Our work proposes a unified upstream regulatory mechanism in which SMARCA4 sustains the NE phenotype through regulation of ASCL1 and NEUROD1 transcriptional programs and concurrently controls REST expression by SRRM4-driven splicing.

SCLC is considered a recalcitrant malignancy, with patients in critical need of novel therapeutic options. A surprising finding of this study is the activation of ERBB/MAPK mitogenic signaling, suppressed in NE-high SCLC, following pharmacological inhibition of SMARCA4/2. Activation of the MAPK pathway

(See figure on next page.)

Fig. 6 SMARCA4/2 inhibition by FHD-286 induces ERBB signaling and sensitivity to afatinib in SCLC. **A** Proliferation curves of SCLC-A, -N, -P and -Y SCLC cell lines treated with FHD-286 for 96 h. The mean \pm SD is shown. **B** Tumor growth of Lx151 and Lx95 SCLC PDXs implanted in NSG mice and treated with 1.5 mg/kg BID p.o. of FHD-286. Student's two-tailed unpaired t test. *** p < 0.001. **C** IPA analysis on significantly upregulated genes in FHD-286-treated cells versus control untreated cells. **D** Immunoblot of ERBB family proteins in H146 and H82 cells after treatment with 100 nM of FHD-286 for 14 days. **E** Western blots of FHD-286 (100 nM) treated cells at the indicated times. **F** Synergy plots of FHD-286 and afatinib in NE SCLC cell lines. **G** Cell death quantification by flow cytometry at day 5 of H146 and H82 cells after treatment with FHD-286, afatinib or both. One way ANOVA followed by Bonferroni comparison test. *** p < 0.001, **** p < 0.0001. **H** Normalized tumor growth of Lx1042 (SCLC-N), Lx1322 (SCLC-P), Lx151 (SCLC-A) and Lx95 (SCLC-A) relative to day 1 of treatment. Two-way ANOVA followed by Bonferroni comparison test. * p < 0.05, ** p < 0.01, **** p < 0.001. **I** Schematic representation of the role of SMARCA4 in sustaining the NE phenotype in SCLC

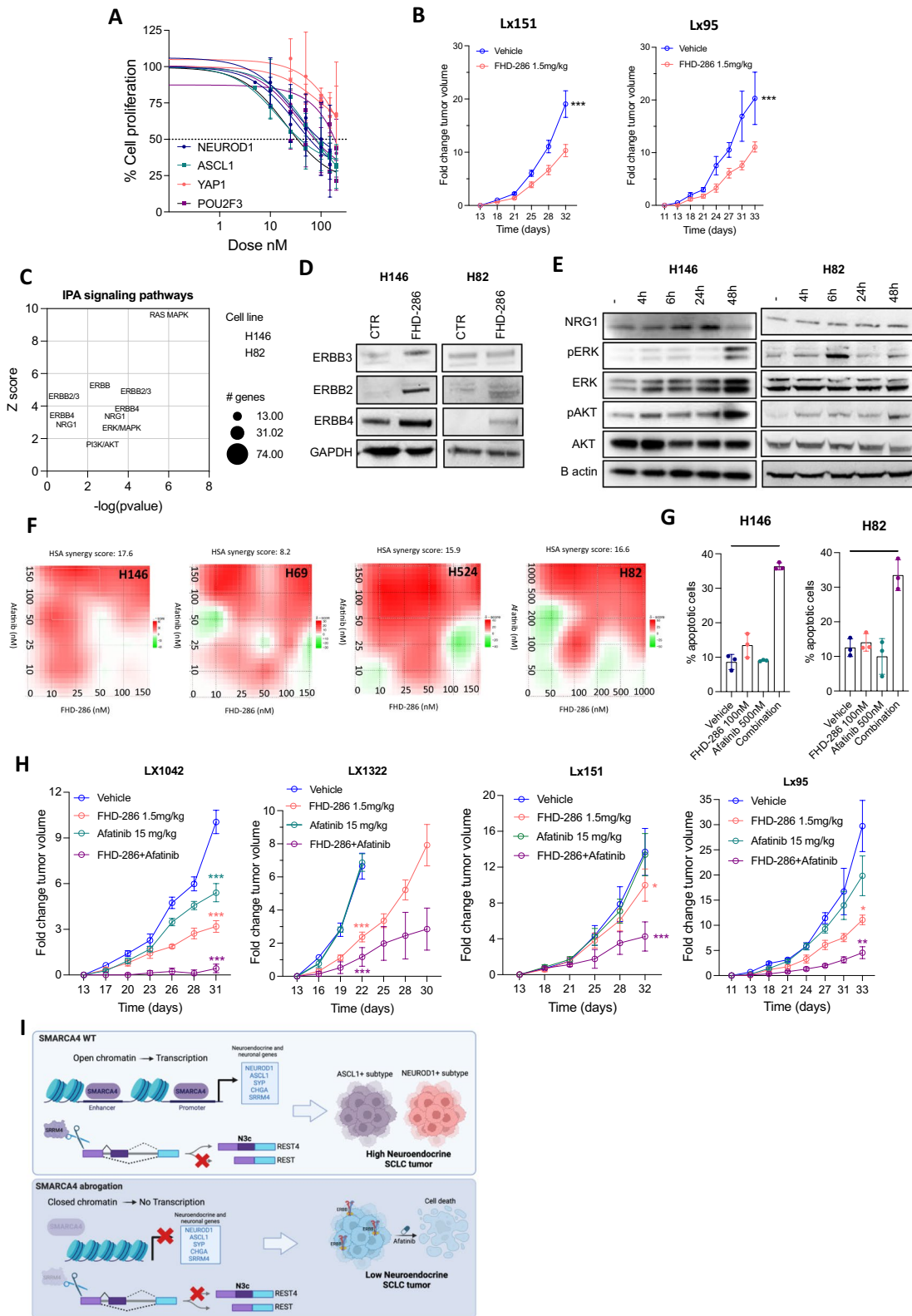


Fig. 6 (See legend on previous page.)

selectively induces cell death of ASCL1+SCLC and reduces the expression of NE markers [71]. ERK activity appears to be limited to low-NE cells in SCLC, in line with the phenotypic changes we observe when SMARCA4 is inhibited [58]. Inactivation of SMARCA4 induced the expression of ERBB family receptors and the cognate ligand NRG1. Consistent with this observation, a previous report showed that SMARCA4 directly regulates NRG1 levels in *Candida albicans* through induction of an antisense NRG1 transcript, suggesting that NRG1 dysregulation by SMARCA4 could be a conserved mechanism [72]. Remarkably, combined SMARCA4/ERBB inhibition showed efficacy in delaying tumor growth, even in PDXs derived from tumors after several lines of treatment, supporting the potential of this combinatorial therapy as a therapeutic strategy for the treatment of SCLC. Our results provide insight into how intrinsic SCLC plasticity is controlled and can be exploited to induce clinically favorable states associated with a therapeutic vulnerability.

Conclusions

In conclusion, our data uncover a critical role for SMARCA4 in sustaining high-NE states in SCLC and define a resulting potential therapeutic vulnerability.

Abbreviations

NE	Neuroendocrine
SCLC	Small cell lung cancer
SCLC-A	Small cell lung cancer-ASCL1
SCLC-N	Small cell lung cancer-NEUROD1
SCLC-P	Small cell lung cancer-POU2f3
SCLC-I	Small cell lung cancer-inflamed
SMARCA4	SWI/SNF related, matrix associated, actin dependent regulator of chromatin, subfamily a, member 4
SMARCA2	SWI/SNF related, matrix associated, actin dependent regulator of chromatin, subfamily a, member 2
NOTCH	Notch receptor
SWI/SNF	SWItch/sucrose non-fermentable
BAF	BRG1/BRM-associated factor
cBAF	Canonical BAF
PBAF	Polybromo-associated BAF
ncBAF	Non-canonical BAF
LUAD	Lung adenocarcinoma
ARID1A	AT-rich interaction domain 1A
mRNA	Messenger RNA
ATPase	Adenosine triphosphatase
ASCL1	Achaete-scute family bHLH transcription factor 1
NEUROD1	Neuronal differentiation 1
SYP	Synaptophysin
FOXA1	Forkhead box A1
FOXA2	Forkhead box A2
INSM1	INSM transcriptional repressor 1
CHGA	Chromogranin A
NCAM1	Neural cell adhesion molecule 1
DLL3	Delta like canonical Notch ligand 3
REST	RE1 silencing transcription factor
REST4	RE1 silencing transcription factor isoform4
NOTCH2	Notch receptor 2
YAP1	Yes1 associated transcriptional regulator
POU2F3	POU class 2 homeobox 3
SRRM4	Serine/arginine repetitive matrix

NRG1	Neuregulin-1
ERBB	Erythroblastic leukemia viral oncogene homologue
HES1	Hes family bHLH transcription factor 1
HEY1	Hes related family bHLH transcription factor with YRPW motif 1
TEAD2	TEA domain transcription factor 2
AJUBA	Ajuba LIM protein
CYR61	Cysteine rich angiogenic inducer 61
WWTR1	WW domain containing transcription regulator 1
Rb1	RB transcriptional corepressor 1
TP53	Tumor protein p53
MYC	MYC proto-oncogene
OTX2	Orthodenticle homeobox 2
GRP	Gastrin releasing peptide
ERK	Extracellular signal-regulated kinase
AKT	AKT serine/threonine kinase 1
ERBB3	Erb-b2 receptor tyrosine kinase 3
EZH2	Enhancer of zeste 2 polycomb repressive complex 2 subunit
LSD1	Lysine-specific histone demethylase 1A
KMD6A	Lysine demethylase 6A
MAPK	Mitogen-activated protein kinases
RTN1	Reticulon1
NRSN1	Neurensin1
MYT1	Myelin transcription factor1
GEMM	Genetically engineered mouse model
GSEA	Gene enrichment analysis
DEG	Differentially expressed genes
CCLC	Cancer cell line encyclopedia
PDX	Patient-derived xenograft
DNA	Deoxyribonucleic acid
5'UTR	Eukaryotic 5' untranslated region
3'UTR	3' untranslated regions
TF	Transcription factor
HOMER	Hypergeometric Optimization of Motif EnRichment
ChIP-seq	Chromatin immunoprecipitation followed by sequencing
ATAC-seq	Assay for transposase-accessible chromatin with sequencing
RNA-seq	RNA sequencing

Supplementary Information

The online version contains supplementary material available at <https://doi.org/10.1186/s13045-024-01572-3>.

Additional file 1.

Additional file 2.

Additional file 3.

Additional file 4.

Additional file 5.

Acknowledgements

We acknowledge the help from the Pathology Core, Gene Editing & Screening Core Facility and Integrated Genomics Operation Core at MSKCC. We thank Foghorn Therapeutics for providing us with FHD-286 for use in this study, and Murphy Hentemann for productive discussions. We thank Abbie Ireland and Dr. Trudy Oliver for providing the processed scRNAseq data. We also acknowledge all members of the Rudin laboratory for their scientific input.

Author contributions

Conceptualization: ER, CMR, AQV; Methodology: ER, HS, YAZ, BPM, HZ, MH, VD, AS, PM, IL, JQ, ES, MA, DB; Data Analysis: ER, YAZ, MA. Writing—Original Draft: ER, AQV, YAZ, CMR; Review & Editing: All authors; Supervision: AQV and CMR; Funding acquisition: CMR and AQV. All authors read and approved the final version of the manuscript.

Funding

This study was supported by Ramon Areces Foundation (to ER), Druckenmiller Center for Lung Cancer Research (to ER, AQV and CMR), NIH T32 CA1600001 (to AQV), American Lung Association (to AQV) NCI R35 CA263816, U24 CA213274, P30 CA008748, the Robert J. and Helen C. Kleberg Foundation, and

the Van Andel Research Institute – Stand Up to Cancer Epigenetics Dream Team (to CMR).

Availability of data and materials

All raw and processed data generated in this study can be found at GEO repository: GSE256345, GSE256346, GSE256347.

Declarations

Ethics approval and consent to participate

All in vivo experiments were performed at Memorial Sloan Kettering Cancer Center (MSKCC) following Animal Care and Use Committee guidelines.

Consent for publication

Not applicable.

Competing interests

AQV has received honoraria from Astra Zeneca. CMR has consulted regarding oncology drug development with AbbVie, Amgen, Astra Zeneca, D2G, Daiichi Sankyo, Epizyme, Genentech/Roche, Ipsen, Jazz, Kowa, Lilly, Merck, and Syros. He serves on the scientific advisory boards of Auron, Bridge Medicines, DISCO, Earli, and Harpoon Therapeutics. All other authors declare no conflicts of interest.

Author details

¹Department of Medicine, Memorial Sloan Kettering Cancer Center, New York, NY, USA. ²Center for Epigenetics Research, Memorial Sloan Kettering Cancer Center, New York, NY, USA. ³Precision Pathology Center, Memorial Sloan Kettering Cancer Center, New York, NY, USA. ⁴Antitumor Assessment Core, Memorial Sloan Kettering Cancer Center, New York, NY, USA. ⁵Weill Cornell Medicine Graduate School of Medical Sciences, New York, NY, USA. ⁶Applied Bioinformatics Core, Weill Cornell Medicine, New York, NY 10065, USA. ⁷Division of Hematology and Oncology, Department of Medicine, Weill Cornell Medicine, New York, NY 10065, USA. ⁸Department of Physiology, Biophysics and Systems Biology, Institute for Computational Biomedicine, Weill Cornell Medicine, New York, NY 10065, USA.

Received: 28 April 2024 Accepted: 3 July 2024

Published online: 30 July 2024

References

- Rudin CM, Brambilla E, Faivre-Finn C, Sage J. Small-cell lung cancer. *Nat Rev Dis Primers*. 2021;7(1):3.
- Rudin CM, Poirier JT, Byers LA, Dive C, Dowlati A, George J, et al. Molecular subtypes of small cell lung cancer: a synthesis of human and mouse model data. *Nat Rev Cancer*. 2019;19:289–97.
- Gay CM, Stewart CA, Park EM, Diao L, Groves SM, Heeke S, et al. Patterns of transcription factor programs and immune pathway activation define four major subtypes of SCLC with distinct therapeutic vulnerabilities. *Cancer Cell*. 2021;39(3):346–60.
- Baine MK, Hsieh MS, Lai WV, Egger JV, Jungbluth AA, Daneshbod Y, et al. SCLC Subtypes Defined by ASCL1, NEUROD1, POU2F3, and YAP1: A comprehensive immunohistochemical and histopathologic characterization. *J Thorac Oncol*. 2020;15(12):1823–35.
- Cai L, De Berardinis RJ, Xie Y, Minna JD, Xiao G. A comparative study of neuroendocrine heterogeneity in small cell lung cancer and neuroblastoma. *Mol Cancer Res*. 2023;21(8):795–807.
- Ireland AS, Micinski AM, Kastner DW, Guo B, Wait SJ, Spainhower KB, et al. MYC drives temporal evolution of small cell lung cancer subtypes by reprogramming neuroendocrine fate. *Cancer Cell*. 2020;38(1):60–78.
- Borromeo MD, Savage TK, Kollipara RK, He M, Augustyn A, Osborne JK, et al. ASCL1 and NEUROD1 reveal heterogeneity in pulmonary neuroendocrine tumors and regulate distinct genetic programs. *Cell Rep*. 2016;16(5):1259–72.
- Mollaoglu G, Guthrie MR, Böhm S, Brägelmann J, Can I, Ballieu PM, et al. MYC drives progression of small cell lung cancer to a variant neuroendocrine subtype with vulnerability to aurora kinase inhibition. *Cancer Cell*. 2017;31(2):270–85.
- Ng J, Cai L, Girard L, Prall OWJ, Rajan N, Khoo C, et al. Molecular and pathologic characterization of YAP1-expressing small cell lung cancer cell lines leads to reclassification as SMARCA4-deficient malignancies. [cited 2024 Jan 31]; Available from: <https://git.biohpc.swmed.edu/BICF/Astrocyte/r>
- Oser MG, Sabet AH, Gao W, Chakraborty AA, Schinzel AC, Jennings RB, et al. The KDM5A/RBP2 histone demethylase represses NOTCH signaling to sustain neuroendocrine differentiation and promote small cell lung cancer tumorigenesis. *Genes Dev*. 2019;33(23–24):1718–38.
- Kiyokawa H, Morimoto M. Notch signaling in the mammalian respiratory system, specifically the trachea and lungs, in development, homeostasis, regeneration, and disease. *Dev Growth Differ*. 2020;62:67–79.
- Shue YT, Drinas AP, Li NY, Pearsall SM, Morgan D, Sinnott-Armstrong N, et al. A conserved YAP/Notch/REST network controls the neuroendocrine cell fate in the lungs. *Nat Commun*. 2022;13(1):2690.
- Centore RC, Sandoval GJ, Soares LMM, Kadoch C, Chan HM. Mammalian SWI/SNF chromatin remodeling complexes: emerging mechanisms and therapeutic strategies. *Trends Genet*. 2020;36(12):936–50. <https://doi.org/10.1016/j.tig.2020.07.011>.
- Mittal P, Roberts CWM. The SWI/SNF complex in cancer—biology, biomarkers and therapy. *Nat Rev Clin Oncol*. 2020;17(7):435–48. <https://doi.org/10.1038/s41571-020-0357-3>.
- Concepcion CP, Ma S, Lafave LM, Bhutkar A, Liu M, Deangelo LP, et al. Smarca4 inactivation promotes LineageSpecific transformation and early metastatic features in the lung. *Cancer Discov*. 2022;12(2):562–85.
- Sun X, Wang SC, Wei Y, Luo X, Jia Y, Li L, et al. Arid1a has context-dependent oncogenic and tumor suppressor functions in liver cancer. *Cancer Cell*. 2017;32(5):574–89.
- Fernando TM, Piskol R, Bainer R, Sokol ES, Trabucco SE, Zhang Q, et al. Functional characterization of SMARCA4 variants identified by targeted exome-sequencing of 131,668 cancer patients. *Nat Commun*. 2020;11(1):5551.
- Navickas SM, Giles KA, Brettingham-Moore KH, Taberlay PC. The role of chromatin remodeler SMARCA4/BRG1 in brain cancers: a potential therapeutic target. *Oncogene*. 2023;42:2363–73.
- Mardinian K, Adashek JJ, Botta GP, Kato S, Kurzrock R. SMARCA4: Implications of an altered chromatin-remodeling gene for cancer development and therapy. *Mol Cancer Ther*. 2021;20:2341–51.
- de Miguel FJ, Gentile C, Feng WW, Silva SJ, Sankar A, Exposito F, et al. Mammalian SWI/SNF chromatin remodeling complexes promote tyrosine kinase inhibitor resistance in EGFR-mutant lung cancer. *Cancer Cell*. 2023;41(8):1516–34.
- Fiskus W, Piel J, Collins M, Hentemann M, Cuglievan B, Mill CP, et al. BRG1/BRM inhibitor targets AML stem cells and exerts superior pre-clinical efficacy combined with BET or Menin inhibitor. *bioRxiv*. 2023; 2023.09.28.560054. <http://biorxiv.org/content/early/2023/10/01/2023.09.28.560054.abstract>.
- Sivakumar S, Moore JA, Montesion M, Sharaf R, Lin DI, Colón CI, et al. Integrative analysis of a large real-world cohort of small cell lung cancer identifies distinct genetic subtypes and insights into histologic transformation. *Cancer Discov*. 2023;13(7):1572–91.
- Alver BH, Kim KH, Lu P, Wang X, Manchester HE, Wang W, et al. The SWI/SNF chromatin remodelling complex is required for maintenance of lineage specific enhancers. *Nat Commun*. 2017 [cited 2024 Jan 31];8. <https://pubmed.ncbi.nlm.nih.gov/28262751/>.
- Quintanal-Villalonga A, Durani V, Sabet A, Redin E, Kawasaki K, Shafer M, et al. Exportin 1 inhibition prevents neuroendocrine transformation through SOX2 down-regulation in lung and prostate cancers. *Sci Transl Med*. 2023;15(707):eadf7006.
- George J, Lim JS, Jang SJ, Cun Y, Ozretia L, Kong G, et al. Comprehensive genomic profiles of small cell lung cancer. *Nature*. 2015;524(7563):47–53.
- Rudin CM, Durinck S, Stawiski EW, Poirier JT, Modrusan Z, Shames DS, et al. Comprehensive genomic analysis identifies SOX2 as a frequently amplified gene in small-cell lung cancer. *Nat Genet*. 2012;44(10):1111–6.
- Quintanal-Villalonga A, Taniguchi H, Zhan YA, Hasan MM, Chavan SS, Meng F, et al. Multiomic analysis of lung tumors defines pathways activated in neuroendocrine transformation. *Cancer Discov*. 2021;11(12):3028–47.

28. Zhang W, Girard L, Zhang YA, Haruki T, Papari-Zareei M, Stastny V, et al. Small cell lung cancer tumors and preclinical models display heterogeneity of neuroendocrine phenotypes. *Transl Lung Cancer Res.* 2018;7(1):32–49.
29. Satija R, Farrell JA, Gennert D, Schier AF, Regev A. Spatial reconstruction of single-cell gene expression data. *Nat Biotechnol.* 2015;33(5):495–502.
30. Langmead B, Salzberg SL. Fast gapped-read alignment with Bowtie 2. *Nat Methods.* 2012;9(4):357–9.
31. Zhang Y, Liu T, Meyer CA, Eeckhoute J, Johnson DS, Bernstein BE, et al. Model-based analysis of ChIP-Seq (MACS). *Genome Biol.* 2008;9(9):1–9.
32. Liao Y, Smyth GK, Shi W. FeatureCounts: an efficient general purpose program for assigning sequence reads to genomic features. *Bioinformatics.* 2014;30(7):923–30.
33. Love MI, Huber W, Anders S. Moderated estimation of fold change and dispersion for RNA-seq data with DESeq2. *Genome Biol.* 2014;15(12):1–21.
34. Thorvaldsdóttir H, Robinson JT, Mesirov JP. Integrative genomics viewer (IGV): high-performance genomics data visualization and exploration. *Brief Bioinform.* 2013;14(2):178–92.
35. Ramírez F, Ryan DP, Grünig B, Bhardwaj V, Kilpert F, Richter AS, et al. deepTools2: a next generation web server for deep-sequencing data analysis. *Nucleic Acids Res.* 2016;44(W1):W160–5.
36. Heinz S, Benner C, Spann N, Bertolino E, Lin YC, Laslo P, et al. Simple combinations of lineage-determining transcription factors prime cis-regulatory elements required for macrophage and B cell identities. *Mol Cell.* 2010;38(4):576–89.
37. Fishilevich S, Nudel R, Rappaport N, Hadar R, Plaschkes I, Stein TI, et al. GeneHancer: genome-wide integration of enhancers and target genes in GeneCards. Database. 2017. <https://doi.org/10.1093/database/bax028>.
38. Welch RP, Lee C, Imbriano PM, Patil S, Weymouth TE, Smith RA, et al. ChIP-Enrich: gene set enrichment testing for ChIP-seq data. *Nucleic Acids Res.* 2014;42(13):e105.
39. Lee CT, Cavalcante RG, Lee C, Qin T, Patil S, Wang S, et al. Poly-Enrich: count-based methods for gene set enrichment testing with genomic regions. *NAR Genom Bioinform.* 2020;2(1):lqaa006.
40. Dobin A, Davis CA, Schlesinger F, Drenkow J, Zaleski C, Jha S, et al. STAR: Ultrafast universal RNA-seq aligner. *Bioinformatics.* 2013;29(1):15–21.
41. Subramanian A, Tamayo P, Mootha VK, Mukherjee S, Ebert BL, Gillette MA, et al. Gene set enrichment analysis: a knowledge-based approach for interpreting genome-wide expression profiles. *Proc Natl Acad Sci USA.* 2005;102(43):15545–50.
42. Yu G, Wang LG, Han Y, He QY. ClusterProfiler: an R package for comparing biological themes among gene clusters. *OMICS.* 2012;16(5):284–287.
43. Liberzon A, Subramanian A, Pinchback R, Thorvaldsdóttir H, Tamayo P, Mesirov JP. Molecular signatures database (MSigDB) 3.0. *Bioinformatics.* 2011;27(12):1739–40.
44. Chen EY, Tan CM, Kou Y, Duan Q, Wang Z, Meirelles GV, et al. Enrichr: Interactive and collaborative HTML5 gene list enrichment analysis tool. *BMC Bioinform.* 2013;14:1–14.
45. Kuleshov MV, Jones MR, Rouillard AD, Fernandez NF, Duan Q, Wang Z, et al. Enrichr: a comprehensive gene set enrichment analysis web server 2016 update. *Nucleic Acids Res.* 2016;44(1):W90–7.
46. Januario T, Ye X, Bainer R, Alicke B, Smith T, Haley B, et al. PRC2-mediated repression of SMARCA2 predicts EZH2 inhibitor activity in SWI/SNF mutant tumors. *Proc Natl Acad Sci USA.* 2017;114(46):12249–54.
47. Gomez AM, Traunmüller L, Scheiffele P. Neurexins: molecular codes for shaping neuronal synapses. *Nat Rev Neurosci.* 2021;22:137–51.
48. Vasconcelos FF, Sessa A, Laranjeira C, Raposo AASF, Teixeira V, Hagey DW, et al. MyT1 counteracts the neural progenitor program to promote vertebrate neurogenesis. *Cell Rep.* 2016;17(2):469–83.
49. Steiner P, Kulangara K, Sarría JCF, Glauser L, Regazzi R, Hirling H. Reticulon 1-C/neuroendocrine-specific protein-C interacts with SNARE proteins. *J Neurochem.* 2004;89(3):569–80.
50. Lee AR, Gan Y, Tang Y, Dong X. A novel mechanism of SRRM4 in promoting neuroendocrine prostate cancer development via a pluripotency gene network. *EBioMedicine.* 2018;35:167–77.
51. Lim JS, Ibaseta A, Fischer MM, Cancilla B, O'Young G, Cristea S, et al. Intratumoral heterogeneity generated by Notch signalling promotes small-cell lung cancer. *Nature.* 2017;545(7654):360–4.
52. Zhang X, Coleman IM, Brown LG, True LD, Kollath L, Lucas JM, et al. SRRM4 expression and the loss of REST activity may promote the emergence of the neuroendocrine phenotype in castration-resistant prostate cancer. *Clin Cancer Res.* 2015;21(20):4698–708.
53. Labrecque MP, Brown LG, Coleman IM, Lakely B, Brady NJ, Lee JK, et al. RNA splicing factors SRRM3 and SRRM4 distinguish molecular phenotypes of castration-resistant neuroendocrine prostate cancer. *Cancer Res.* 2021;81(18):4736–50.
54. Ito T, Udaka N, Yazawa T, Okudela K, Hayashi H, Sudo T, et al. Basic helix-loop-helix transcription factors regulate the neuroendocrine differentiation of fetal mouse pulmonary epithelium. *Development.* 2000;127(18):3913–21.
55. Neptune ER, Podowski M, Calvi C, Cho JH, Garcia JGN, Tudor R, et al. Targeted disruption of NeuroD, a proneural basic helix-loop-helix factor, impairs distal lung formation and neuroendocrine morphology in the neonatal lung. *J Biol Chem.* 2008;283(30):21160–9.
56. Osada H, Tomida S, Yatabe Y, Tatematsu Y, Takeuchi T, Murakami H, et al. Roles of achaete-scute homologue 1 in DKK1 and E-cadherin repression and neuroendocrine differentiation in lung cancer. *Cancer Res.* 2008;68(6):1647–55.
57. Bohuslavova R, Fabriciova V, Smolik O, Lebrón-Mora L, Abaffy P, Benesova S, et al. NEUROD1 reinforces endocrine cell fate acquisition in pancreatic development. *Nat Commun.* 2023;14(1):55546.
58. Calbo J, van Montfort E, Proost N, van Drunen E, Beverloo HB, Meuwissen R, et al. A functional role for tumor cell heterogeneity in a mouse model of small cell lung cancer. *Cancer Cell.* 2011;19(2):244–56.
59. Nguyen EM, Taniguchi H, Chan JM, Zhan YA, Chen X, Qiu J, et al. Targeting lysine-specific demethylase 1 rescues major histocompatibility complex class I antigen presentation and overcomes programmed death-ligand 1 blockade resistance in SCLC. *J Thorac Oncol.* 2022;17(8):1014–31.
60. Mahadevan NR, Knelson EH, Wolff JO, Vajdi A, Saigi M, Campisi M, et al. Intrinsic immunogenicity of small cell lung carcinoma revealed by its cellular plasticity. *Cancer Discov.* 2021;11(8):1952–69.
61. Duplaquet L, Li Y, Booker MA, Xie Y, Olsen SN, Patel RA, et al. KDM6A epigenetically regulates subtype plasticity in small cell lung cancer. *Nat Cell Biol.* 2023;25(9):1346–58.
62. Chan JM, Quintanal-Villalonga Á, Gao VR, Xie Y, Allaj V, Chaudhary O, et al. Signatures of plasticity, metastasis, and immunosuppression in an atlas of human small cell lung cancer. *Cancer Cell.* 2021;39(11):1479–96.
63. Pozo K, Kollipara RK, Kelenis DP, Rodarte KE, Ullrich MS, Zhang X, et al. ASCL1, NKX2-1, and PROX1 co-regulate subtype-specific genes in small-cell lung cancer. *iScience.* 2021;24(9):102953.
64. He T, Xiao L, Qiao Y, Klingbeil O, Young E, Wu XS, et al. Targeting the mSWI/SNF complex in POU2F-POU2AF transcription factor-driven malignancies. *bioRxiv: the preprint server for biology.* 2024.
65. Leslie Duplaquet KS, Alexander WYing XLYLXQRL. Mammalian SWI/SNF complex activity regulates POU2F3 and constitutes a targetable dependency in small cell lung cancer. *bioRxiv.* 2024.
66. Olsen RR, Ireland AS, Kastner DW, Groves SM, Spainhower KB, Pozo K, et al. ASCL1 represses a SOX9+ neural crest stem-like state in small cell lung cancer. *Genes Dev.* 2021;38(11–12):847–69.
67. Flores-Morales A, Bergmann TB, Lavallee C, Batth TS, Lin D, Lerdrup M, et al. Proteogenomic characterization of patient-derived xenografts highlights the role of REST in neuroendocrine differentiation of castration-resistant prostate cancer. *Clin Cancer Res.* 2019;25(2):595–608.
68. Puca L, Vlachostergios PJ, Beltran H. Neuroendocrine differentiation in prostate cancer: emerging biology, models, and therapies. *Cold Spring Harb Perspect Med.* 2019;9(2):a030593.
69. Li Y, Donmez N, Sahinalp C, Xie N, Wang Y, Xue H, et al. SRRM4 drives neuroendocrine transdifferentiation of prostate adenocarcinoma under androgen receptor pathway inhibition. *Eur Urol.* 2017;71(1):68–78.
70. Shimajo M, Shudo Y, Ikeda M, Kobashi T, Ito S. The small cell lung cancer-specific isoform of RE1-silencing transcription factor (REST) is regulated by neural-specific Ser/Arg repeat-related protein of 100 kDa (nSR100). *Mol Cancer Res.* 2013;11(10):1258–68.
71. Caesar R, Hulton C, Costa E, Durani V, Little M, Chen X, et al. MAPK pathway activation selectively inhibits ASCL1-driven small cell lung cancer. *iScience.* 2021;24(11):103224.
72. Cleary IA, Lazzell AL, Monteagudo C, Thomas DP, Saville SP. BRG1 and NRG1 form a novel feedback circuit regulating *Candida albicans* hypha formation and virulence. *Mol Microbiol.* 2012;85(3):557–73.

Publisher's Note

Springer Nature remains neutral with regard to jurisdictional claims in published maps and institutional affiliations.